PERFORMANCE STUDY ON TURBULENT HEAT TRANSFER USING RECTANGULAR AIR DUCT INTEGRATED WITH CONTINUOUS AND INTERMITTENT RIBS TURBULATORS

Sarah NASHEE *, Khudheyer S. MUSHATET

Department of Mechanical-engineering, College of engineering, University of Thi-Qar, Thi-Qar, 64001, Iraq

* Corresponding author; E-mail: sara.rabee@utq.edu.iq

To continue the scientific path specialized in enhancing the thermal performance of thermal systems, several tests are carried out to improve the overall performance of a rectangular duct as air flows through it. This study reports experimentally and numerically the heat transfer enhancement and overall performance of a rectangular air duct with various arrangement of continuous and intermittent ribs turbulators. The ribs are inserting in several array arrangements at a 90^o relative to the direction of flow. Three ribs lengths s= 30, 60 and 150 mm employed with the several arrangements that's tested in the current study, with the pitch ratios (p/e)= 5.0 and height ratios (e/H) = 0.330. These cases include: continuous ribs case (CR), intermittent-continuous-intermittent ribs case (ICIR) and intermittent-ribs (IR). Reynolds number (Re) is ranging from 10,000 to 35,000. The experimental work was performed by designed and fabricated test rig while the numerical work was performed in commercially ANSYS Fluent 17.2. the outcomes show that (IR) case offers the best overall performance for all tested velocities, its 1.54 for experimental study and 1.57 for numerical study at Re=10000. Also, the highest friction factor values are found in (IR) case, it is found to be 0.082 in Re=10000.

Key words*: overall performance, intermittent ribs, continuous ribs, friction factor*

1. Introduction

A variety of cooling techniques have been developed recently to guarantee the maximum levels of internal heat transmission in numerous thermal applications. Enhancing heat transfer through engineering research is important and beneficial since it increases the efficiency of heating systems like heat exchangers. Considerable economic and technical savings are possible with the appropriate heat transfer technique. The design of thermal applications requires high thermal performance methodologies, which has raised interest in developing ways to increase heat transfer coefficients[1,3]. Ribs turbulaturs have efficient impact of many thermal applications such as cooling of evaporators, spacecraft radiators, air conditioning systems, and gas turbine blades. [4,5]. Researchers conducted extensive experimental and analytical studies to improve thermal performance and confirmed that obstructions in the flow path lead to an increase in the turbulence intensity of the fluid flow. Passive methods generally involve inserting fins, fins, baffles, depressions, wires, etc. into the flow path to increase the heat transfer rate [4,5]. Researchers conducted extensive experimental and analytical studies to improve thermal performance and confirmed that obstructions in the flow path lead to an increase in the turbulence intensity of the fluid flow. Passive methods generally involve inserting fins, fins, baffles, depressions, wires, etc. into the flow path to increase the heat transfer rate [6-8]. .One of the most important passive techniques for increasing heat transfer is the employing of ribs turbulators. The main effect of the presence of ribs is volume reduction and cost reduction. Periodic fins are often employed to improve the heat transfer process in various cooling channels. In general, turbulent flow in channels with continuous and regularly arranged transverse fins is often used as a simple model to study the influence of roughness on heat transfer and friction coefficient properties[9]. The presence of ribs creates a complex flow field such as separation, reattachment, and relaxation in the mainstream flow, resulting in a strong secondary flow [10-12]. An Le [13] presented a study using two systems to perform heat transfer and pressure drop. One of the rigs has two channels, one with aspect ratio (1/8) and the other with aspect ratio (1/4). (Re)was between 3000 and 13000. This test shows that, square ribs produce the highest heat transfer improvement. They found that thermal performance decreased as the Reynolds number raised. The heat transfer enhancements of a square channel roughened with ribs parallel to two opposing walls were studied by Rallabandi et al. [14]. (p/e) in the range of 5 to 10 was applied. The range of (Re) that were examined was 30,000–400,000. The results of the experiment demonstrated that, even with a bigger pressure drop, the heat transfer coefficient raised with raising of e/D_h and p/e. Yang [15] conducted an investigation to look into the pressure loss and thermal performance in a square channel that have blocking ribs roughened. In this study, (Re) between 1400 and 4500. There was a range of 5 to 15 in (p/e). The experimental findings demonstrated that ribs enhanced the heat transfer. Also, Bagabir et al. [16] presented a numerical study of the turbulent heat transfer characteristics of finned square channels. (Re)was varies between 10^4 and 4×10^4. The ribs were inclined at a 45° angle, arranged in series and staggered at the top and bottom of the channel. The results showed that the heat transfer improvement in channels was generally 230–580% greater than in the case of smooth channels. Yongsiri et. al. [17] presented a numerical study testing the heat transfer in channels with separated ribs. (Re)varied between 4,000 and 24,000. The heat transfer and pressure drop were tested. The results show that at high values of (Re), the inclined fins with $\theta = 60°$ and 120° achieved higher thermal performance than other angles. (p/e)of 10 had the greatest heat transfer coefficient. Boga [18] studied the effects of heat transfer and flow field in square channels with different fin geometries (rectangular, semicircular, and triangular). Inlet Re number changed from 5,000to10,000. All ribs were placed in a channel with (p/e) = 4. The findings demonstrated that, for (Re) under consideration, the heated wall's (Nu) is greatest in the channel with triangle ribs. Additionally, a computational fluid dynamics (CFD) simulation was carried out by Farooqui [19] to calculate the heat transfer in a rectangular channel. (Re) was varied between 5000 and 24000. The outcomes showed that the presence of ribs increases heat transfer compared to smooth channels. Shukla [20] A study was carried out to improve the heat transfer in square channels provided by different types of fins. Experimental data were also made 4 rib arrangements were used: continuous attachment ribs, continuous separation ribs, break attachment thin ribs, and break attachment thick ribs. (Re) from 10,000 to 30,000 and p/e = 10 were tested The damaged rib was fixed at a 90° angle, and (e/D_h) was 0.15, 0.10, and 0.08125. Researchers found that the standard k-ε model produced better results compared to other models studied. Jennifer et. al. [21] conducted a study to increase the heat transfer coefficient. The ribs utilize the internal cooling channels of the turbine blades. (p/e) was 8. It was numerically demonstrated that ribs rised the turbulence level of the flow, resulting in increased heat transfer compared to a wall without fins. Etminan et al. [22] presented a simulation to study heat transfer in straight, convergent, and divergent channels using square ribs at the top and bottom of the channel. (Re) range from $7*10^4$ to 10^5 was investigated. They discovered that, in comparison to the straight channel, the divergent channel's thermal efficiency rises by about 18%. The current research deals with the effect of the ribs on the path of air passing at a flow inside a rectangular channel where (Re) ranges from 10,000 to 35,000 tests is conducted to exam channel with presence of ribs in several arrangements with (p/e)= 5.0 and (e/H) = 0.3.

2. Experimental setup

The testing rig is designed and constructed to fulfill the requirements of the research endeavor. It consists of the parts displayed in Figures 1 and 2, which represent the schematic design and picture of the test rig, respectively. The rectangular channel was built from a piece of galvanized iron that measured 2 mm in thickness. The dimensions of the channel are length (L=100 cm), width (W=15cm), and height (H=6cm). Installing rib in the channel can improve heat transfer between the heated surface and the electrified fluid, which will improve performance. Seven rows of ribs are arranged in a straight line perpendicular to the direction of air flow. Examine values of (p/e) =5 and (e/H) 0.33. Three rib lengths of s 30, 60and 150 mm are tested in different configurations. As in Fig.3.

Figure 1. The photograph view of the test rig

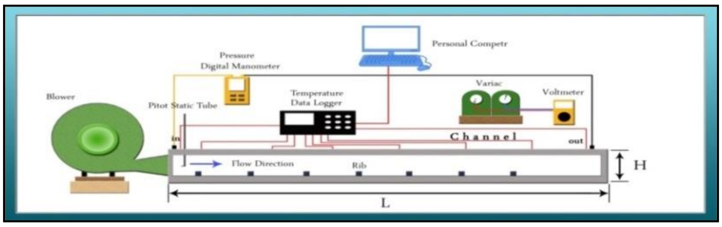

Figure 2. The schematic diagram of test rig

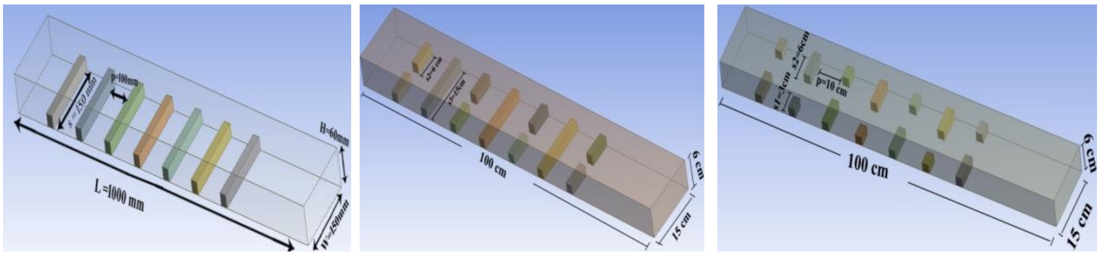

a **b** **c**

Figure 3. The configurations of the ribs cases a-CR case, s=150 mm; b-ICIR case, s= 150,60 mm; c-IR case, s= 60, 30 mm

3. Numerical analysis

The geometry consists of a 3D rectangular channel with ribs turbulator arranged in parallel one by one. In this section, Three cases for ribs arrangements array are considered. The first case is continuous rectangular ribs on the lower surface of the channel (CR), the second is intermittent-continuous-intermittent ribs (ICIR), and the third is intermittent ribs(IR). The numerical analysis carried out utilizing ANSYS Fluent 17.2 software to simulate three-dimensional turbulent airflow and heat transfer characteristics in the roughed channel.

3.1 Mesh construction

To achieve discretization in space, the flow field must be divided into smaller control volumes. Control volumes of many shapes, including hexahedral and tetrahedral control volumes, can be created, as well as structured or unstructured grids. The tetrahedral mesh is utilized as shown in Fig. 4 because it is effective for the separation flow. It is clear that the mesh is incredibly small around the walls and around the ribs in order to capture the flow behavior in these regions.

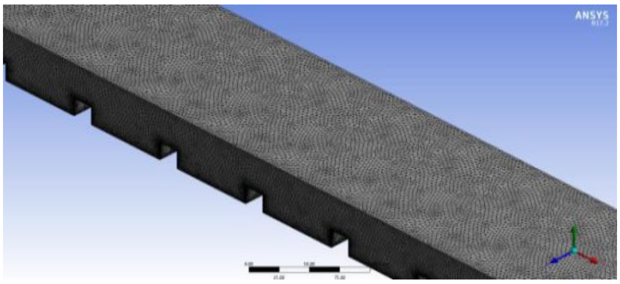

Figure 4. The considered mesh generation

3.2 Grid independency

The geometry must be divided into cells that contain a mesh in order to model the fluid flow problem using computational fluid dynamics. Choosing the ideal grid size is crucial to getting precise

Table 1. Different grids and their (Nu) and (f) for different studied cases at Re= 20,000

The case	No. of elements	Nu	$Nu_{deviation}$	f	$f_{deviation}$
CR:(p/e)=5, (e/H)=0.33, s= 150 mm	2,210,733	92.0123	0.0142	0.0563	0.014
	2,344,658	90,684	0.0126	0.0571	0.0086
	2,412,236	89.559	0.0085	0.0576	0.0068
	2,549,349	88,782		0.058	
ICIR:(p/e)=5,(e /H)=0.33, s= 150, 60 mm	2,465,253	91.66	0.1207	0.068	0.037
	2,486,390	92.78	0.0059	0.071	0.035
	2,524,667	93.34	0.0051	0.074	0.011
	2,579,547	93.82		0.075	
IR:(p/e)=5, (e/H)=0.33,s= 60, 30 mm	2,577,377	100.832	0.0213	0.08	0.036
	2,627,738	103.204	0.01	0.083	0.024
	2,747,589	101.98	0.0094	0.081	0.012
	2,810,848	102.88		0.082	

results. In order to determine the proper grid size for running numerical simulations over a variety of (Re), tests of grid independence were conducted. (Nu) and (f) were ascertained by performing the grid independence test at Re= 20,000. Table (1) provides a summary of the findings and displays the designated grid for each form and arrangement.

3.3 Governing equations

The Navier-Stokes, the energy, and the continuity equations are used to analyze turbulent flow:

Equation of continuity [23]

$$\frac{\partial u}{\partial x} + \frac{\partial v}{\partial y} + \frac{\partial w}{\partial z} = 0 \tag{1}$$

x, y, z components of conservation of momentum[23]

$$u\frac{\partial u}{\partial x} + v\frac{\partial u}{\partial y} + w\frac{\partial u}{\partial z} = -\frac{1}{\rho}\frac{\partial P}{\partial x} + \frac{\mu}{\rho}\left(\frac{\partial^2 u}{\partial x^2} + \frac{\partial^2 u}{\partial y^2}\right) \tag{2}$$

$$u\frac{\partial v}{\partial x} + v\frac{\partial v}{\partial y} + w\frac{\partial w}{\partial z} = = -\frac{1}{\rho}\frac{\partial P}{\partial y} + \frac{\mu}{\rho}\left(\frac{\partial^2 v}{\partial x^2} + \frac{\partial^2 v}{\partial y^2}\right) \tag{3}$$

$$u\frac{\partial w}{\partial x} + v\frac{\partial w}{\partial y} + w\frac{\partial w}{\partial z} = -\frac{1}{\rho}\frac{\partial P}{\partial z} + \frac{\mu}{\rho}\left(\frac{\partial^2 w}{\partial x^2} + \frac{\partial^2 w}{\partial y^2} + \frac{\partial^2 w}{\partial z^2}\right) \tag{4}$$

Energy equation [23]

$$u\frac{\partial T}{\partial x} + v\frac{\partial T}{\partial y} = \alpha\left(\frac{\partial^2 T}{\partial x^2} + \frac{\partial^2 T}{\partial y^2}\right) \tag{5}$$

Air was used as the working fluid. The next portion present the necessary equations to calculate the variables.

The net heat input to the fluid was specified from the electrical energy input to the system as follows:

$$Q = V.I \tag{6}$$

The mean heat transfer coefficient (**$\bar{h}$**) is calculated by the following expression [24]**:**

$$\bar{h} = \frac{Q}{A_s\,(T_w - T_b)} \tag{7}$$

The mean wall temperature is attained[25]. wall temperature at the channel's bottom surface is Tw_n.

$$T_w = \frac{1}{n}\sum T_{wn} \tag{8}$$

The following procedures lead to the mean bulk temperature (Tb) [26]:

$$T_b = \frac{\int_0^L\int_0^H\int_0^W \rho\ c_p\,uT\,dx\,dy\,dz}{\int_0^L\int_0^H\int_0^W \rho\,u\,dx\,dy\,dz} \tag{9}$$

The mean Nusselt number (**Nu**) is estimated as follows [27]:

$$Nu_{avg.} = \frac{\bar{h}\,.D_h}{k} \tag{10}$$

$D_h = \frac{4\,A_c}{C}$, Ac=W.H, C=2(W+H), where A_C is the cross section area of the channel and C is the circumference.

The average friction factor Friction factor can be obtained by the following expression [28]

$$f = \frac{\Delta P}{\frac{1}{2}\rho\, u_{avg.}^{2}} \cdot \frac{D_h}{L} \tag{11}$$

The entire performance, or thermal-hydrodynamic performance, is computed as follows [29]:

$$\eta = (Nu_w/Nu_o)/(f_w/f_o)^{1/3} \tag{12}$$

3.4 The standard *k*-*ε* model

One of the models that is most frequently used is the standard k-ε model. Two equations comprise this semi-empirical model: one for the transit of turbulent kinetic energy (k) and another for the dissipation of turbulent kinetic energy (ε). The model's derivation is predicated on the turbulence of the flow and the minimal effects of molecular viscosity. Consequently, the conventional model can only be applied to turbulent flows.

For turbulent kinetic energy (***k***) [30]:

$$\rho\left(\frac{\partial}{\partial x}(ku) + \frac{\partial}{\partial y}(kv) + \frac{\partial}{\partial z}(kw) \right) = \frac{\partial}{\partial x}\left(\frac{\mu_t}{\sigma_k}\frac{\partial k}{\partial x}\right) + \frac{\partial}{\partial y}\left(\frac{\mu_t}{\sigma_k}\frac{\partial k}{\partial y}\right) + \frac{\partial}{\partial z}\left(\frac{\mu_t}{\sigma_k}\frac{\partial k}{\partial z}\right) + G - \rho\varepsilon \tag{13}$$

For energy dissipation rate (**ε**) [30]:

$$\rho\left(\frac{\partial}{\partial x}(\varepsilon u) + \frac{\partial}{\partial y}(\varepsilon v) + \frac{\partial}{\partial z}(\varepsilon w) \right) = \frac{\partial}{\partial x}\left(\frac{\mu_t}{\sigma_\varepsilon}\frac{\partial \varepsilon}{\partial x}\right) + \frac{\partial}{\partial y}\left(\frac{\mu_t}{\sigma_\varepsilon}\frac{\partial \varepsilon}{\partial y}\right) \frac{\partial}{\partial z}\left(\frac{\mu_t}{\sigma_\varepsilon}\frac{\partial \varepsilon}{\partial z}\right) + \rho\,\frac{\varepsilon}{k}\,G - C_{1\varepsilon}\,\rho\,\frac{\varepsilon}{k} \tag{14}$$

Where G is referred to the generation term and is given [30]:

$$G = \mu_t\left[2\left(\frac{\partial u}{\partial x}\right)^2 + 2\left(\frac{\partial v}{\partial y}\right)^2 + 2\left(\frac{\partial w}{\partial z}\right)^2 + \left(\frac{\partial v}{\partial y}\frac{\partial u}{\partial x}\right)^2 + \left(\frac{\partial v}{\partial z}\frac{\partial w}{\partial x}\right)^2 + \left(\frac{\partial v}{\partial z}\frac{\partial w}{\partial y}\right)^2\right] \tag{15}$$

3.5 Boundary condition

A partial differential equation requires a few more conditions to be satisfied in order to find a suitable solution and get the desired outcomes. At the inlet: w=v=0. At pipe wall P=0. At outlet u=v=w=0. Smooth exit for dependent variable ($\partial u/\partial x = \partial v/\partial y = \partial w/\partial z = 0$) are assumed.

4. Results and discussions

4.1 The experimental research

Three cases with the presence of rib turbulators are introduced, (CR), (ICIR), and (IR). Pitch to rib height ratio (P/e) = 5 and (e/H) = 0.33. As in Fig.5, (CR) case, the (IR) case and the (ICIR) case are compared. The values of the highest Nusselt numbers are based at (IR), where the average (Nu) values for the (IR) case increased by 13% when compared to the (CR) case, 7% when compared to the (ICIR) case, and 27% when compared to the smooth channel. This rise can be attributed to the fact that two recirculating regions at the intermittent first rib are distorted by a recirculating part of the flow. This complex flow is passing at the second continuous rib and the forming one recirculating region. This region combines with the main flow and then the process reached intermittent third rib. The process is repeated for the other downstream ribs. As a result, there are more recirculating zones and mixing with the hot surface, which enhances heat transfer. The rise in heat transfer in the presence of ribs is responsible for the increase in the Nusselt number because, in each case, the ribs contributed more to the fluid's recycling and mixing than the smooth channel did. This improvement in heat transfer also led to an increase in the rate of heat transfer because the obstacles created a recycling area and increased fluid turbulence. The behavior is the same in all cases—an rise in the value of Nusselt with increased flow velocity—but the values vary because each arrangement can produce greater vortices and remixing in a different way than the others.

The (IR) case has the greatest values of friction factor as a comparison with the other cases and that for all the considered Reynolds number values. This is because of the change in the shape of the blockages versus the flowing stream and consequently increases the surface resistance and as expected due to the suppression of the viscous sub-layer. This leads to the pressures drop rise, thus increasing the (f) values. Fig. 6 displays the differences. The aforementioned case gives the highest friction as a result of the increase in the fluid mixing rate and the formation of the largest vortices among the other cases that were compared with it, and this resulting disturbance caused a greater drop in pressure in this case, which caused this drop to increase in of friction factor according to the equation of the friction factor. in the three cases' outcomes.

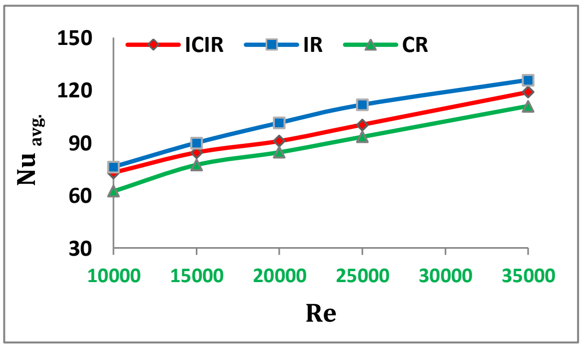

Figure 5. The Nusselt number variation with (Re) for (IR), (CR), and (ICIR) cases

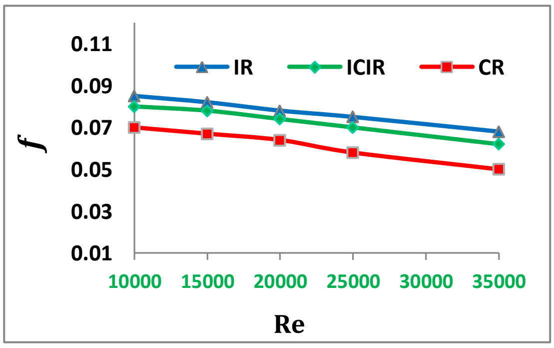

Figure 6. The variation of the friction factor with(Re) for (IR), (CR) and (ICIR) cases

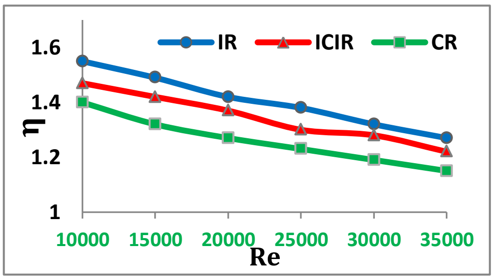

Figure 7. The variation of the overall performance for (IR), (CR) and (ICIR) cases

In Figure 7 it has been observed that when (Re) rises, (η) falls. When compared to the other cases, the arrangement of (IR) scenario yields the highest values of overall performance. The outcomes showed that there was a 12% rise in overall performance for (IR) case when compared to (CR) and a 9% increase when compared to the (ICIR). The reason of rising (η) for this case is due to the enhancement of the heat transfer due to the arrangement method that allowed the difference in the size and location of the vortices formed that led to rise heat transfer.

In fact, the performance gradually decreases as (Re) rises, i.e. the flow velocity rise. This was happened in all cases. the enhancement in heat transfer as (Re) increasing is slower, because that the flow has not the sufficient time to interchange the heat transfer with rib turbulators and consequently the enhancement in the overall performance decrease.

4.2 The comparison between the experimental and numerical studies

Figure 8 compares (Nu) experimental and numerical outcomes gained for the case of the channel that fitted with (CR) ribs,. The both results have average deviations of 7%. Figure.11 displays the agreements between the results for (f), with average deviations of 12%. Regarding the situation of (ICIR), average variations of 6% are obtained by comparing the numerical and experimental results of (Nu), as shown in Fig. 9. In contrast, (f) (as in Fig.12) have average variations of 7%. Fig. 10 compares the (Nu) results for (IR). There was an agreement between the results with average deviation does not exceed 6%. With regard to the (f), Fig. 13 an average deviation of 8%.

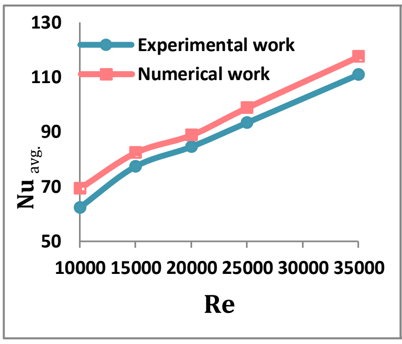

Figure 8. The experimental and numerical works for (Nu) and CR case

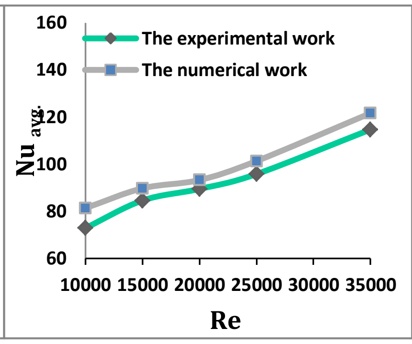

Figure 9. The experimental and numerical works for (Nu) and ICIR case

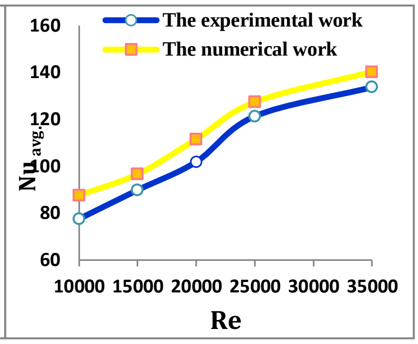

Figure 10. The experimental and numerical works for (Nu) and IR case

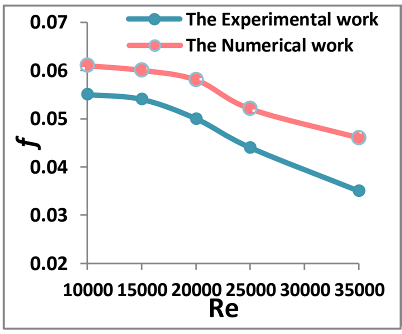

Figure 11. The experimental and numerical works for (*f*) and CR case

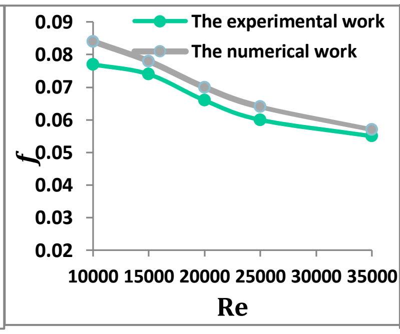

Figure 12. The experimental and numerical works for (*f*) and ICIR case

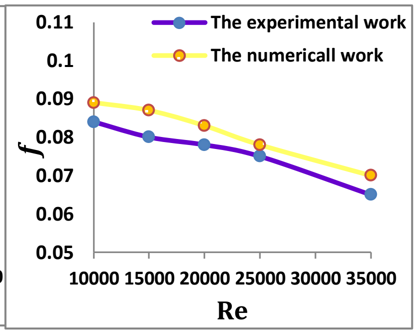

Figure 13. The experimental and numerical works for (*f*) and IR case

4.3 Empirical correlations

For every scenario in this work, empirical correlations between (f)and (Nuavarage)have been performed using the experimental data that was gathered. The form of this analysis is obtained by using the XLSTAT software. In the case of continuous ribs, the first correlation is for varying pitch ratios and rib turbulators' heights. The empirical equations are shown in Eqs. 16 and 17.

For the ribs rows in odd position $C1 = A_{r1}/A_c$, for the ribs rows in the even position $C2= A_{r2}/A_c$, where A_c = W*H, A_{r1} = s*e (for the ribs rows in the odd position), A_{r2} = s*e (for the ribs rows in the even position), where A_{r1} is obstruction area of ribs row in the odd position, A_{r2} is obstruction area of ribs row in the even position. For $10000 \leq Re \leq 35000$:

$$Nu = 1.23562\, (C1)^{0.04597}\, (C2)^{-0.243}\, P_r^{0.4}\, Re^{0.46093} \tag{16}$$

$$f = 9.633354\, (C1)^{-0.21862}\, (C2)^{-0.56202}\, P_r^{0.4}\, Re^{-0.40867} \tag{17}$$

For the (Nu) and (*f*), the differences between empirical correlations and experimental values are within 3% and 2%, with (Re) values under consideration, as in Figs. 14 and 15, where (p/e)=5 and (e/H)= 0.3.

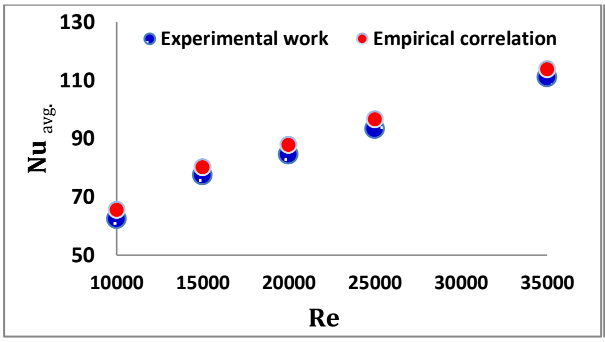

Figure 14. The experimental results of (Nu) and empirical correlations for (CR)

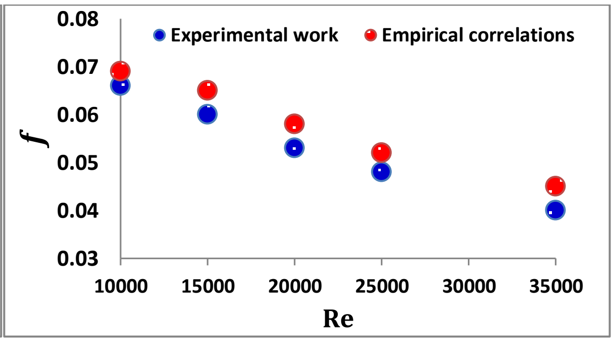

Figure 15. The experimental results of (f) and empirical correlations for (CR)

The second case is (ICIR) case, whereas correlation Eqs. 18 and 19 are calculating depending upon the obstruction ratios made by the rib turbulators, which represent the ratio between the areas of obstruction to the surface area of the channel as below. For $10000 \leq Re \leq 35000$:

$$Nu = 1.1412\, C_1^{-0.448}\, C_2^{0.09392}\, P_r^{0.4}\, Re^{0.40727} \tag{18}$$

$$f = 0.13763\, C_1^{-1.7702}\, C_2^{0.54742}\, P_r^{0.4}\, Re^{-0.2267} \tag{19}$$

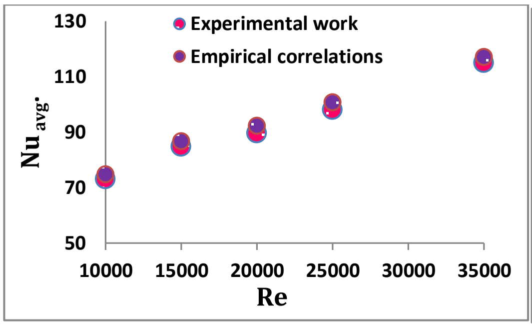

Figure 16. The experimental results and empirical correlations of (Nu) for(ICIR)

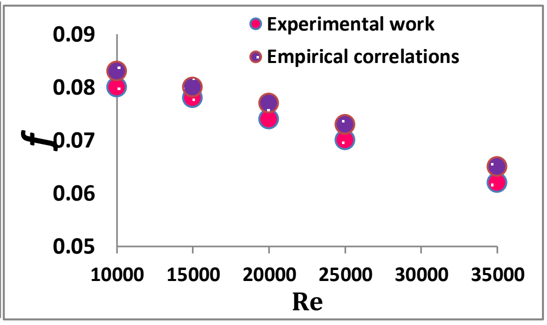

Figure 17. The experimental results and empirical correlations of (*f*) for (ICIR)

For the (Nu) and friction factor the highest variances between the predicted and experimental results are within 3% and 2%. These differences are explained in Figs. 16 and 17 by using the (ICIR).

In the third case of (IR), the rib provide obstruction ratios that are used in correlation equation calculations. where, stands for the ratio of the obstruction's area to the channel's surface area. Eqs. 20 and21 show an empirical correlation of (Nu)and(f). For $10000 \leq Re \leq 35000$:

$$Nu = 3.0597\, C_3^{-0.2085}\, C_4^{0.4432}\, P_r^{0.4}\, Re^{0.3557} \tag{20}$$

$$f = 1.139\, C_3^{-0.222}\, C_4^{0.64442}\, P_r^{0.4}\, Re^{-0.273} \tag{21}$$

For (Nu) and (f) the highest differences between the expected and actual values are within 3% and 2%. These discrepancies are illustrated in Figs.18 and19 employing the (IR) example for the (Re) under consideration.

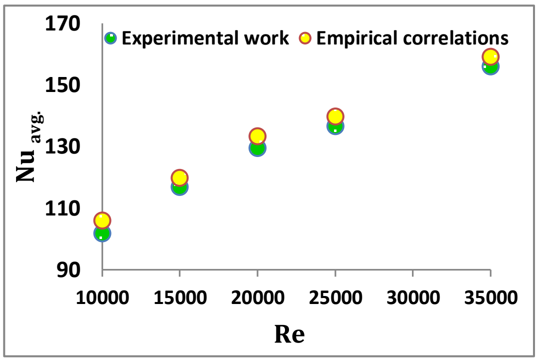

Figure 18. The experimental results and empirical correlations of (Nu) for (IR)

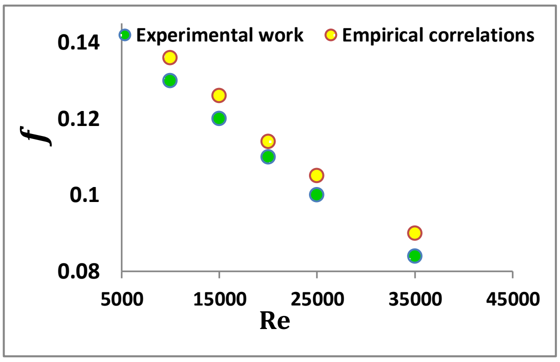

Figure 19. The experimental results and empirical correlations of (*f*) for (IR)

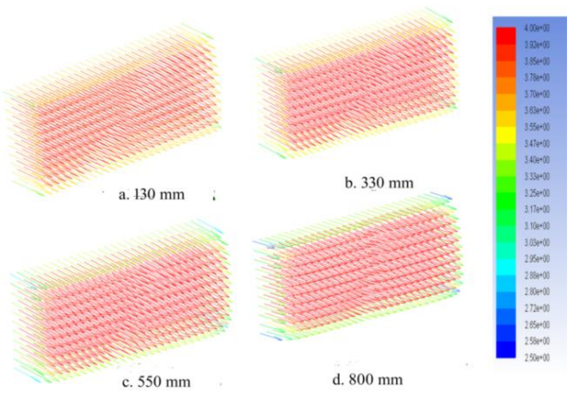

Figure 20. Velocity vector for the smooth channel for Re=20000

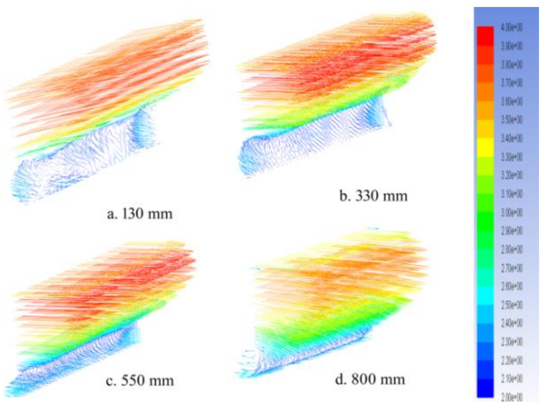

Figure 21. Velocity vector for the CR ribs case for Re=20000

The velocity vectors of smooth duct and with ribs present are illustrated in Figs. 20-22. There are recirculation zones following every obstacle. The core's high velocity is caused by the reduction of the core stream space at this region. The fluid's separation at the ribs' surface when it passes through them creates incredibly intricate vortices, particularly at (IR).

For air flowing with Re = 20,000, the presented results through the figures were for cross-sections at axial locations, 130 mm, 330 mm, 550 mm and 800 mm, frames (a to d).

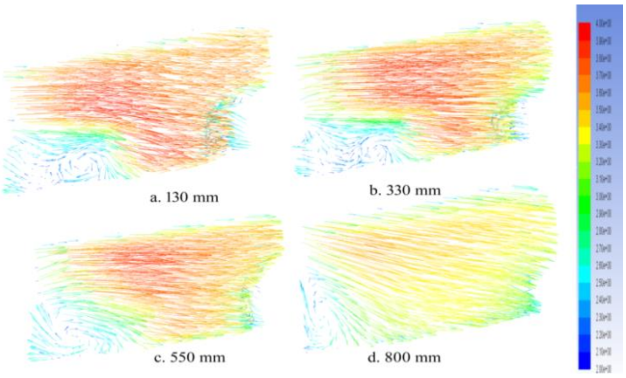

Figure 22. Velocity vector for (IR) case for Re=20000

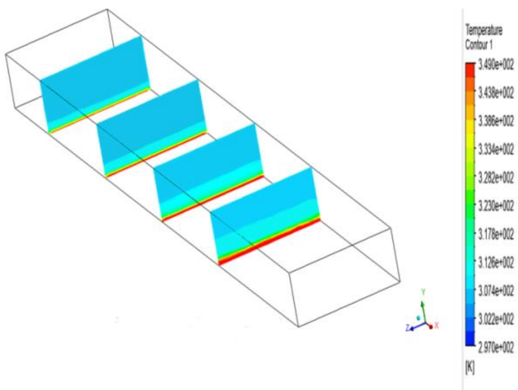

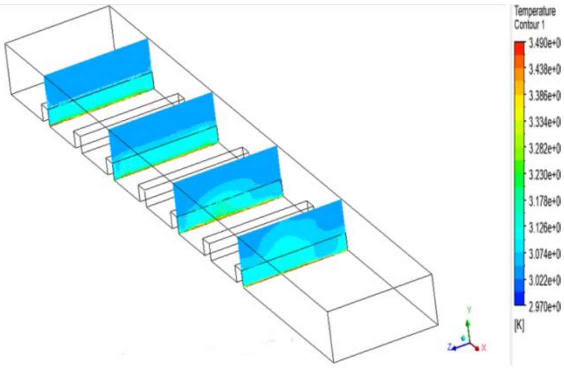

Figure 23. Temperature-contour for smooth channel for Re=20000

Figure 24. Temperature-contour for (CR) for Re=20000

Figures. 23, 24, and 25 show the curve of temperature. The lack of circulation flow causes the fluid temperature to gradually drop from the lower to the higher portion of the channel wall. The fluid's temperature will rise as it moves downstream from the first position of 120 mm to the positions of 320 mm, 520 mm, and 720 mm. This will cause the fluid to draw more heat from the channel wall and cause the thermal boundary layer to grow, which will cause the colder area at the upper of the channel to get smaller and smaller.

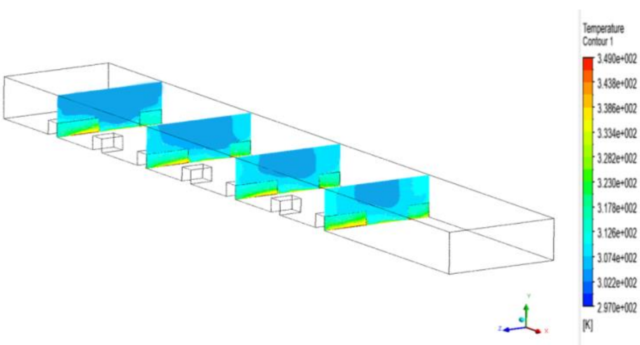

Figure 25. Temperature -contour for (IR) case for Re=20000

The channel's temperature distribution will be disturbed by the addition of rib turbulators. Just as the vortex flow prevents the hydrodynamic boundary layer from growing uniformly, it will also prevent the thermal boundary layer from developing uniformly.

5. Conclusion

The impact of three different arrangement was studied for turbulent flow of air through a channel. The outcomes give a several conclusion:

1. In general, the outcomes indicate that the (Nu) with velocity in all cases tested, and it was clear in the case of (IR). This is due to the raised in mixing of the air, which provided a greater opportunity for heat exchange due to the formation of larger vortices and a rising in the recirculation area. The maximum Nu for case (IR) was discovered at Re=35,000.

2. As the Re raises from 10000 to 35000, the channel's overall performance at the three cases is decreasing. Furthermore, the outcomes indicates that case (IR) give the maximum overall performance at Re=5000, its 1.54 for experimental study and 1.57 for numerical study.

3. Compared to continuous ribs (CR), the friction factor rises while employing the intermittent-continuous-intermittent ribs instance (ICIR) for all Reynolds values and it’s have the greater values at (IR) case.

4. At Re = 10,000 and Re = 35,000, the highest friction factor for using the (IR) configuration is found to be 0.082 and 0.063, respectively.

5. As the Reynolds number rise from 10000 to 35000, the channel's overall performance at the intermittent-continuous-intermittent ribs scenario (ICIR) decreases from 150% to 98%.

6. The results of the numerical work in general showed slightly higher values than the theoretical results due to the standard conditions in which the numerical work is carried out compared to laboratory experiments.

Nomenclature

A	amplitude of the wavy wall [m]
D_h	hydraulic diameter [m]
e	obstacle height [m]
f	friction factor [-]
h	convective heat transfer coefficient, [W/(m^2. K)]
K	coefficient of thermal conductivity, [W/(m. K)]
L	length of channel [m]
Nu	Nusselt number [-]
p	pitch of ribs [m]
Re	Reynolds number [-]
s	length of ribs [m]
T	temperature [K]
t	ribs thickness [m]

References

[1] Sharma, N., *et al*., Detailed heat transfer and fluid flow investigation in a rectangular duct with truncated prismatic ribs, *Experimental Thermal and Fluid Science*, *96* (2018), pp. 383-396

[2] Prajapati, A. N., Tariq, A., Detailed heat transfer characteristics of matrix cooling channels with rib angle 35° using liquid crystal thermography, *Proceedings*, Gas Turbine India Conference, American Society of Mechanical Engineers, 2019, Vol. 83525

[3] Yadaba, M., Senapati, J., R., Implementation of hybrid rib-turbulators on the thermal performance of solar air heater duct: a collective review, *Sustainable Energy Technologies and Assessments*, *52* (2022), 102345.

[4] Khaled, R. A., Mushatet, K. S., CFD analysis for a twisted elliptical double tube heat exchangers integrated with a twisted tape, *International Journal of Heat and Technology*, *41* (2023), 5, pp. 1301-1308

[5] Nashee, S. R., Enhancement of heat transfer in nanofluid flow through elbows with varied cross-sections: A computational study, *International Journal of Heat and Technology*, *42* (2024), 1, pp. 311-319

[6] Ali, Z. K., Mushatet, Kh. S., Intensification of turbulent heat transfer in a circular tube by inserting different configuration of finned converging-diverging nozzles turbulators, *University of Thi-Qar Journal for Engineering Sciences*, *11.1* (2020), pp. 1-7

[7] Mushatet, Kh., Nashee, S., Experimental and computational investigation for 3-D duct flow with modified arrangement ribs turbulators, *Thermal Science*, *25*, (2021), 3A, pp.1653-1663

[8] Al-Jibory, M. W., *et al*., An experimental investigation of heat transfer enhancement in elliptical passage fitted with different rib geometries, *International Journal of Mechanical Engineering and Technology*, *9* (2018), 13, pp.1033-1048

[9] Tamang, *et al*., A novel concept for a rib turbulator for optimizing the cooling performance in a square channel, *International Journal of Heat and Mass Transfer*, *221* (2024), pp.125144

[10] Lee, M., Ahn, S., Heat transfer and frictions in the rectangular divergent channel with ribs on one wall, *International Journal of Aeronautical and Space Sciences*, *17.3* (2016), pp. 352-357

[11] Sattar, E. A., *et al*., Enhancement heat transfer in shell and tube heat exchanger by used hybrid and nanofluid, *AIP Conference Proceedings*, Vol. 2787. No. 1. AIP Publishing, 2023

[12] Nashee, S. R., *et al*., Numerical investigation of flow in vertical rectangular channels equipped with three different obstacles shape, *AIP Conference Proceedings*, Fourth International Conference On Advances In Physical Sciences And Materials: Icapsm 2023, 17–18 August 2023,Coimbatore, India. (2024), Vol. 3122, Issue 1

[13] Le, A., The Effect of Heat Transfer Coefficient on High Aspect Ratio Channel Accompanied By Varying Rib Aspect Ratio, Electronic Theses and Dissertations, University of Central Florida, 2009, 4103

[14] Rallabandi, A. P., *et al*., Heat transfer and pressure drop correlations for square channels with 45 degree ribs at high Reynolds number, *ASME J. Heat Transfer*, *131* (2009), 071703

[15] Yang, W., Xue, S., Experimental investigation on heat transfer characteristics of high blockage ribs channel, *Proceedings*, 12th International Conference on Heat Transfer, Fluid Mechanics and Thermodynamics, 2016, pp. 1165–1172

[16] Bagabir, A. M., *et al*., Turbulent periodic flow and heat transfer in a square channel with different ribs, *CFD Letter*, *5* (2013), pp. 67–80

[17] Yongsiri, K., *et al.*, Case studies in thermal engineering augmented heat transfer in a turbulent channel flow with inclined detached-ribs, *Case Stud. Therm. Eng.*, *3* (2013), pp. 1–10

[18] Boga, V., Jayavel, S., Numerical simulation of heat transfer in channels with different ribs, *International Journal of Mechanical and Production Engineering*, *2* (2014), 12, pp. 79–82

[19] Farooque, M. R., Numerical study on effect of rectangular shaped ribs arranged in different patterns on thermal performance of a solar air heater duct, Ph. D. thesis, National Institute Of Technology Rourkela, Rourkela, India, 2015

[20] Shukla, A. K., Dewan, A., Computational study of heat transfer enhancement through broken and continuous attached ribs in a square channel, First International ISHMT-ASTFE Heat and Mass Transfer Conference (IHMTC), Thiruvananthapuram, India, Dec. 2015

[21] Jennifer, J. E., *et al.*, Analysis of turbine blade cooling using ribs 1, *International Journal of Advances in Science Engineering and Technology*, *3* (2015), pp. 57–61

[22] Bader, N. M., Mushatet, Kh. S., Thermal performance improvement of artificially roughened solar air heater, *Engineering Review*, *43* (2023), 1, pp. 66-88

[23] Mushatet, Kh., Bader, N., Thermal performance assessment for the solar air collector integrated with ribs turbulators under Nassiriya city climate, *Journal of Mechanical Engineering Research and Developments*, *45* (2022), pp. 166-174.

[24] Oztop, H. F., *et al*., Analysis of turbulent flow and heat transfer over a double forward facing step with obstacles, *International Communications in Heat and Mass Transfer*, *39* (2012), 9, pp. 1395-1403

[25] Mushatet, Kh. S., Bader, N. M., Experimental investigation for the performance of the solar air dryer with vortex generator, *Defect and Diffusion Forum*, *419* (2022), Trans Tech Publications, Ltd., pp. 57–67

[26] Hamood, H. M., *et al*., Numerical investigation to study the effect of three height of triangular obstacles on heat transfer of nanofluids in a microchannel, *International Review of Mechanical Engineering*, *17* (2024), 11, pp. 533-540

[27] Nashee, S. R., Numerical study for fluid flow and heat transfer characteristics in a corrugating channel, *International Journal of Heat and Technology*, *41* (2023), 2, pp. 392-398

[28] Rishack, Q. A., *et al*., Numerical investigation of non-newtonian fluids flow in two direction double step square expansion, Wasit - Kut, Iraq, 2018 International Conference on Advance of Sustainable Engineering and its Application (ICASEA), IEEE, 2018, pp. 210-214

[29] Nashee, S. R., Numerical simulation of heat transfer enhancement of a heat exchanger tube fitted with single and double-cut twisted tapes, *International Journal of Heat and Technology*, 42 (2024), 3, pp. 1003-1010

Received: 30.04.2024.
Revised: 26.07.2024.
Accepted: 02.08.2024.